PROCEEDINGS B

rspb.royalsocietypublishing.org

Research

Cite this article: Hol FJH, Rotem O, Jurkevitch E, Dekker C, Koster DA. 2016 Bacterial predator–prey dynamics in microscale patchy landscapes. *Proc. R. Soc. B* **283**: 20152154. http://dx.doi.org/10.1098/rspb.2015.2154

Received: 7 September 2015
Accepted: 18 January 2016

Subject Areas:
microbiology, ecology, biophysics

Keywords:
Bdellovibrio bacteriovorus, metapopulation, nanofabricated landscapes, predator–prey

Author for correspondence:
Daniel A. Koster
e-mail: danikoster@gmail.com

Electronic supplementary material is available at http://dx.doi.org/10.1098/rspb.2015.2154 or via http://rspb.royalsocietypublishing.org.

THE ROYAL SOCIETY PUBLISHING

Bacterial predator–prey dynamics in microscale patchy landscapes

Felix J. H. Hol[1], Or Rotem[2], Edouard Jurkevitch[2], Cees Dekker[1] and Daniel A. Koster[3]

[1]Department of Bionanoscience, Kavli Institute of Nanoscience, Delft University of Technology, Lorentzweg 1, 2628 CJ Delft, The Netherlands
[2]Department of Agroecology and Plant Health, The Robert H. Smith Faculty of Agriculture, Food and Environment, The Hebrew University of Jerusalem, Jerusalem, Israel
[3]Department of Ecology, Evolution and Behavior, The Alexander Silberman Institute of Life Sciences, The Hebrew University of Jerusalem, Edmond J. Safra Campus, Jerusalem 91904, Israel

FJHH, 0000-0001-8061-0826; DAK, 0000-0003-2129-1233

Soil is a microenvironment with a fragmented (patchy) spatial structure in which many bacterial species interact. Here, we explore the interaction between the predatory bacterium *Bdellovibrio bacteriovorus* and its prey *Escherichia coli* in microfabricated landscapes. We ask how fragmentation influences the prey dynamics at the microscale and compare two landscape geometries: a patchy landscape and a continuous landscape. By following the dynamics of prey populations with high spatial and temporal resolution for many generations, we found that the variation in predation rates was twice as large in the patchy landscape and the dynamics was correlated over shorter length scales. We also found that while the prey population in the continuous landscape was almost entirely driven to extinction, a significant part of the prey population in the fragmented landscape persisted over time. We observed significant surface-associated growth, especially in the fragmented landscape and we surmise that this sub-population is more resistant to predation. Our results thus show that microscale fragmentation can significantly influence bacterial interactions.

1. Introduction

Bacterial habitats, such as soil, our gastrointestinal tract, and even the ocean are spatially structured at the microscale [1,2]. Soil typically contains particles with sizes that vary between 2 µm or less for clay and 1 mm for sand [3,4] (figure 1*a*). It is within the confines of the interconnected cavities in between soil particles that microorganisms, such as bacteria, interact. Most of our knowledge of population dynamics in such highly structured landscapes comes from a large body of theoretical [5–7] and experimental studies [8–11] concerning macroscopic organisms in macroscopic landscapes. Due to technical challenges, however, experimental study and even a clear theoretical framework of the population dynamics of microorganisms in spatially structured microhabitats such as soil is lacking, especially for interacting bacterial populations such as predator–prey communities.

One may hypothesize that for bacteria, a landscape with constrictions with a size of only a few micrometres can be considered fragmented. This hypothesis predicts that the population dynamics differ significantly between individual patches and that the dynamics of interacting bacteria at the local (patch) level become decorrelated quickly with increasing distance [12]. Habitat fragmentation may also influence the lifetime of the population as a whole [5,8,12,13]. However, bacteria differ in important ways from 'large' animals: bacteria grow to higher densities, possibly reducing stochastic fluctuations that may lead to local extinction. Bacteria are also highly mobile, in terms of their swimming speed [14] as well as in terms of their ability to pass through small constrictions [15]. Furthermore, while diffusion of signalling molecules, food, and waste is very efficient

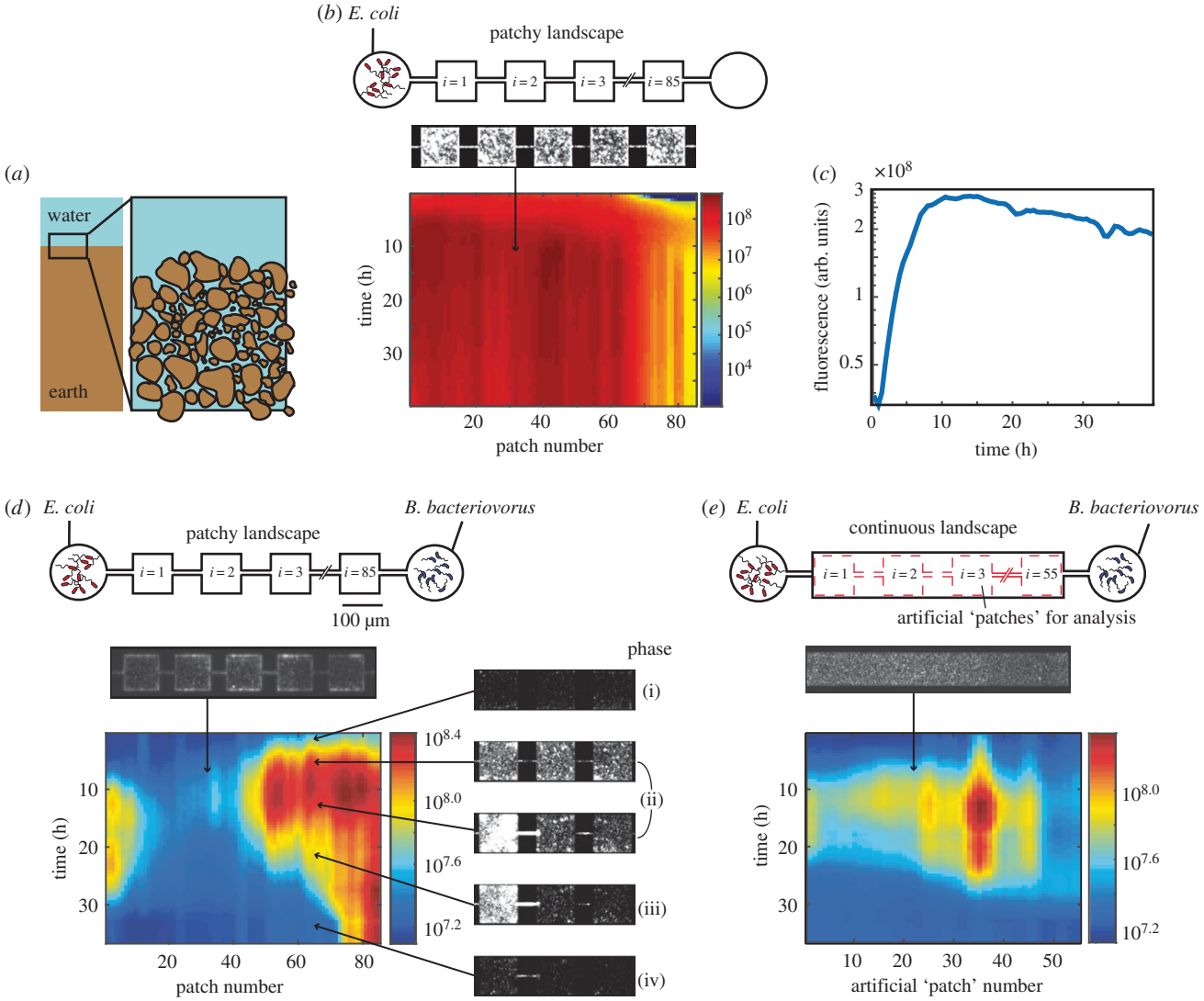

Figure 1. On-chip predator–prey system. (*a*) Soil consists of a three-dimensional network of micrometre-sized patches. (*b*) A control experiment, in which only prey is introduced to a patchy landscape, consisting of coupled patches (top). A heatmap of a kymograph (depicting space horizontally and time vertically, the colour bar indicates logarithmically scaled fluorescent intensity in arbitrary units) showing the population dynamics of fluorescently labelled *E. coli*. (*c*) The mean prey growth dynamics over all patches shows the familiar phases of bacterial growth: exponential phase and entry into stationary phase (at $t = 10$ h). (*d*,*e*) Predator–prey dynamics in the presence of predator in a patchy landscape (*d*) and a 'continuous' landscape (*e*). Software-generated 'virtual' patches that are used in data analysis of the continuous habitat are indicated by red dashed lines. In both habitats there initially is a steep rise in fluorescence which corresponds to the growth of *E. coli*, followed by a death phase in which *E. coli* lyse after predation. Each pixel represents a single habitat patch. Microscopy images show representative snapshots of the population dynamics in phases (i)–(iv), arrows indicate the approximate space and time of image acquisition.

at microscopic scales, diffusion at larger scales is negligible. Finally, bacteria can adopt very different lifestyles, living clustered together in biofilms with greatly reduced mobility, or as motile planktonic individuals [16]. For these reasons, it is unclear whether bacterial habitats that are spatially structured at the microscale can be considered 'fragmented' or not. Because macroscopic fragmentation has been shown to affect key parameters such as the global lifetime of a population [8–11], we believe there is reason to assume that microscopic fragmentation could be of importance for understanding bacterial life in natural structured habitats such as soil. However, the question of how fragmentation affects predator–prey dynamics at the microscale has remained unanswered.

Over the past few years, microfabrication techniques have allowed for the creation of microscale synthetic ecosystems that are structured at the spatial scales relevant to bacterial populations [17–21]. It thus has become technically feasible to quantify bacterial predator–prey interactions in each of the individual micrometre-scale patches of a landscape under controlled conditions over many generations. Taking advantage of these recent advances, we fabricated a microscale fragmented habitat and a non-fragmented habitat and contrasted bacterial predator–prey dynamics in these two habitat types. We studied the bacterial predator *Bdellovibrio bacteriovorus* preying upon *Escherichia coli*. *Bdellovibrio bacteriovorus* is a small (0.4×1 µm) and highly motile (it can swim over 160 µm s^{-1}, or 160 body lengths per second [22]) predator of Gram-negative bacteria, that occurs, for example, in soil, in the human gut and in water [23]. To complete its life cycle, *B. bacteriovorus* inserts itself into the periplasmic space of its prey and converts it into a round-shaped 'bdelloplast' [24]. *Bdellovibrio bacteriovorus* subsequently extracts and ingests solutes from its prey and increases in length, after which it divides and four to six progeny are produced per *E. coli* prey. Approximately 3–4 h after invasion, *B. bacteriovorus* lyses its host and swims away to hunt for the next prey [23]. While

B. bacteriovorus are ferocious predators, a small fraction of prey may survive predation due to plastic phenotypic resistance, preventing the total eradication of the prey population [25].

Studying the *B. bacteriovorus*–*E. coli* interaction in both fragmented and continuous landscapes allows us to test the hypothesis that a bacterial habitat featuring microscale constrictions is fragmented and as such influences the predator–prey interaction. Specifically, we address the question to what extent a spatially structured microhabitat gives rise to variations in predation rates, and at what scale predator–prey dynamics are spatially correlated in a microstructured landscape such as soil. Can *B. bacteriovorus* predate effectively in spatially structured landscapes? Does fragmentation increase the persistence of the prey population? Furthermore, given that *B. bacteriovorus* has shown potential to protect crops and reduce biofouling [26–29], it would be useful to know how its effectiveness in structured habitats relates to its effectiveness as measured in well-mixed (unstructured) culture flasks [30–32]. In this regard, *B. bacteriovorus* has also attracted significant interest because of its potential to eradicate bacterial biofilms which are spatially structured at the microscale [33,34].

2. Material and methods

(a) Strains and growth conditions

(i) Growth of *Escherichia coli*

We used strain JEK 1036 previously described in [18], which is wild-type *E. coli* W3110 labelled with a green fluorescent protein (lacZY::GFPmut2). JEK 1036 was grown overnight (O/N) from glycerol in Luria-Bertani (LB) broth at 30°C whilst shaken at 200 r.p.m., diluted 1 000-fold the next morning in Diluted Nutrient Broth (DNB, 0.8 g l^{-1} NB, 2 mM $CaCl_2 \cdot 2H_2O$, 3 mM $MgCl_6 \cdot 2H_2O$, pH 7.6) and grown to $OD_{600} \sim 1$. Fluorescence expression was induced by adding 100 µM of isopropyl β-D-1-thiogalactopyranoside (IPTG, Promega) to the medium.

(ii) Growth of *Bdellovibrio bacteriovorus* and microhabitat inoculation

Escherichia coli JEK 1036 [18] was cultivated to maximum turbidity ($OD_{600} \sim 4$) in LB broth, then concentrated to $OD_{600} = 10$ by centrifugation and subsequently resuspended in HEPES buffer (25 mM HEPES, 2 mM $CaCl_2 \cdot 2H_2O$, 3 mM $MgCl_6 \cdot 2H_2O$, pH 7.8). *Bdellovibrio bacteriovorus* HD100, with a chromosomal fusion of the HuaA histone-like protein gene [24] to monomeric Teal protein (mTeal), was added to this medium from glycerol stock and was incubated O/N in a volume of 2 ml while shaking at 280 r.p.m. at 28°C, until a transparent liquid was obtained. The culture's transparency indicates that all *E. coli*, except for a fraction that is phenotypically resistant, have been lysed. The culture was then spun down at 3 000 r.p.m. for 10 min and resuspended in 2 ml fresh DNB, at 28°C. The microhabitat was simultaneously inoculated with approximately 3 µl of resuspended *B. bacteriovorus* culture and approximately 3 µl of pure *E. coli* culture in DNB medium in a 1 : 1 ratio (measured by optical density) from opposite sides.

(b) Experimental set-up

(i) Microfabrication of microhabitats

To emulate the patchy geometry of natural bacterial habitats with relevant spatial dimensions (figure 1*a*), and to allow for the quantitative study of predator–prey interactions as a function of space and time, we created a well-defined linear array of habitat patches on a silicon chip, that are connected to each other by narrow corridors (figure 1*b*,*d*, top) [18,35]. As a control for the patchiness of the patchy geometry, we also designed a continuous landscape of identical volume that consisted of one large habitat without internal constrictions (figure 1*e*). Microhabitats were fabricated in silicon using a two-step procedure of photolithography and reactive ion etching following a previously published protocol [18,35]. The patchy microhabitats consisted of 85 patches (each 100 µm in length, 100 µm in width, and 15 µm in depth) connected by corridors (50 × 5 × 15 µm), the continuous microhabitats consisted of a single patch (8 500 × 100 × 15 µm) with a total volume identical to the volume of the patchy habitat. The 180 nm deep slits are too shallow for the passage of bacteria and thus preclude them from leaving the microhabitats and entering the reservoirs. On the other hand, the slits do allow for the diffusion of, for example, nutrients and waste [18,35]. At the start of an experiment, the reservoirs (having a volume approx. 15 times the habitat) were filled with fresh DNB medium (supplemented with 100 µM IPTG) to ensure that plenty of nutrients were available to the *E. coli* for the entire duration of the experiment. Two ports to inoculate bacteria were drilled through the silicon, one at each end of the habitat, furthermore, ports were drilled to allow for the filling of the reservoirs. After short exposure to O_2-plasma to facilitate proper bonding, a silicon microhabitat was bonded to a polydimethylsiloxane (PDMS) coated coverslip. The microhabitats and reservoirs were then filled with fresh DNB medium (supplemented with 100 µM IPTG). Subsequently, cultures of *B. bacteriovorus* and *E. coli* were inoculated from opposite ends as described above. The medium in the device was not replenished during the experiment. After the habitat and reservoirs had been filled and the habitat had been inoculated with bacteria, the inlet holes were sealed with quick-drying PDMS. Data were acquired for periods up to 3 days, the exact duration of each experiment is shown on the time axis of the relevant figures. All experiments were performed in triplicate.

(ii) Microhabitat imaging

To capture the dynamics of the prey population in the presence (and absence) of the predator, microhabitats were imaged every 20 min using an Olympus IX81 inverted microscope controlled with MicroManager v. 1.4.14 software [36], equipped with a 20× 0.75 numerical aperture (NA) objective, an Andor Neo sCMOS camera and a motorized stage (Marzhauser). The sample was illuminated using an X-cite 120 Q (Lumen dynamics) light source. We used the total fluorescence intensity in the GFP channel as a proxy for prey density which was previously shown to be a valid approach [35,37]. Due to the limited brightness of *B. bacteriovorus*, predator cells were not continuously monitored. The fluorescent mTeal fusion, however, allowed us to periodically verify the presence of *B. bacteriovorus* using a 100× objective. The set-up was enclosed in an incubator set to 28°C.

(iii) Image processing and data analysis

Images were processed in Matlab using a custom script. Briefly, each patch was subdivided in 98 × 98 regions (we left out a margin from the edges of the patches to remain unbiased by the limited precision of the microscope stage movement) from which fluorescence time traces were obtained by binning into bins of 3 × 3 pixels. By dividing the patches into subregions, we are able to quantify the variation of predation rates *within* individual patches (see Results), while the binning reduces noise in the fluorescence signal. To render the analysis of the continuous landscape as comparable as possible to the patchy landscape, artificial 'virtual patches' of identical size and inter-patch spacing were computationally generated in the continuous landscape during analysis (figure 1*b*). In designing the habitat geometries, we chose to keep the total habitat volume of the

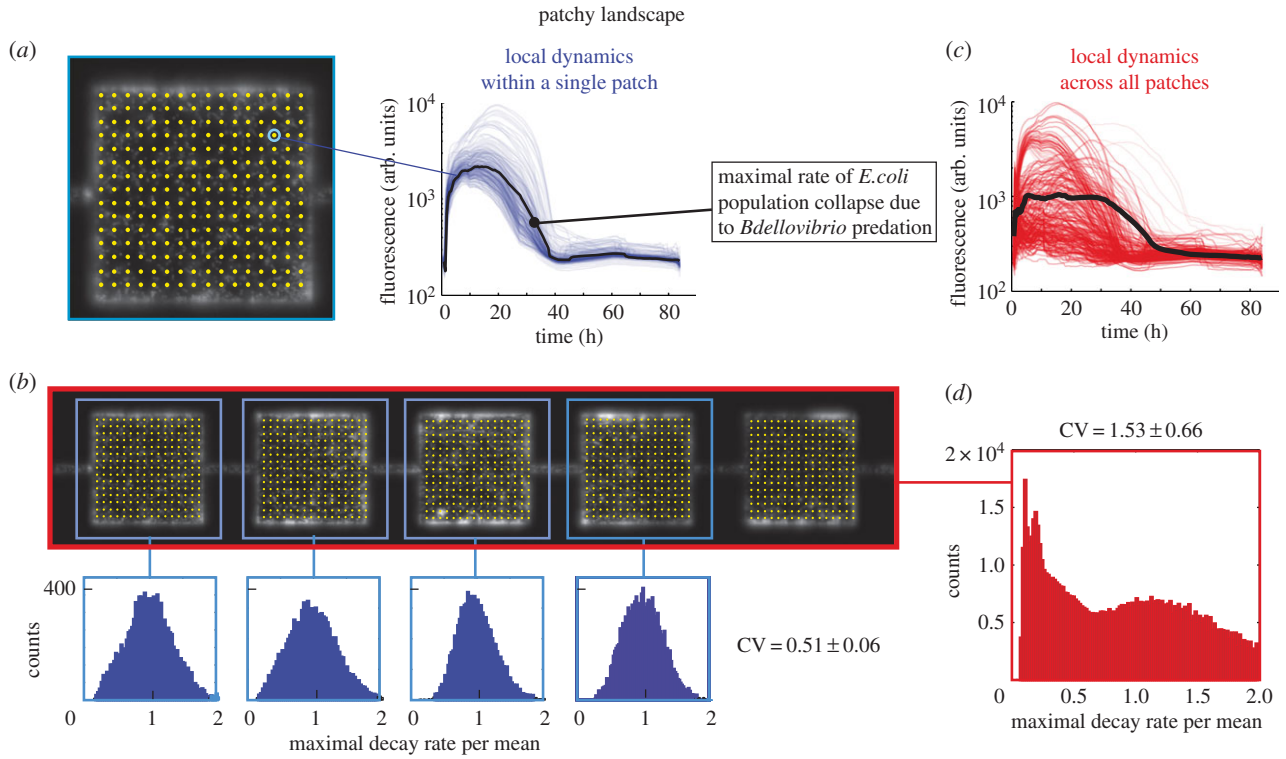

Figure 2. Predation rates in a patchy landscape. (*a*) Yellow dots indicate 98 × 98 points (for clarity, only 16 × 16 are shown) that were used to generate time traces (thin blue lines show single time traces for one patch, the fat black line represents the mean) from patches of the fragmented landscape. The maximum predation rate is extracted from individual traces. (*b*) Distribution of the maximal rate of decay of four patches. (*c*) All time traces of all patches within a patchy habitat (thin red lines show single time traces for one patch, the fat black line represents the mean). (*d*) The distributions of the maximum decay rates calculated for all points in all patches within the patchy landscape.

patchy and continuous landscapes identical, and therefore, given the different geometries of the two landscapes, the continuous landscape consisted of 55 'virtual patches' versus 85 patches for the patchy landscape. Next, we performed a background correction for each time trace and smoothed the time traces using a five-point window. Subsequently, the maximal predation rates were calculated for each time trace by calculating the maximal negative slope (maximal predation rate) beyond the maximum value of a time trace (figures 2*a* and 3*a*). Using this algorithm, each of the patches yields 10^4 values for the maximal predation rates. We exclude time traces originating from empty regions within the patch (typically a few per cent of the traces, defined by a maximum that is 10% or less than the most frequent maximal value of all time traces in the patch). The values for the maximal predation rates were then plotted in histograms such as the blue histograms in figures 2*b* and 3*b*. To usefully compare the variance of this distribution between patches, also in cases where the mean values differ, we divided the maximal predation rate by its mean. We thus describe the variation as the coefficient of variation (CV), defined as the standard deviation of the distribution divided by the mean of the distribution. The within-patch CV thus obtained for each patch was averaged over all patches yielding two values: one for all of the patches in the patchy geometry ($CV_{l,p}$), and one for all of the 'virtual patches' in the continuous geometry ($CV_{l,c}$). To compare the local CV of the patches with the CV of the landscape as a whole, we generated two more numbers: one that described the global CV for the entire landscape for a patchy geometry ($CV_{g,p}$) and one that described the global CV of the entire landscape for the continuous geometry ($CV_{g,c}$). The degree to which the global CV for the entire landscape and that of the individual patches (local CV) differ is expressed in terms of their ratio R according to $R =$ Global CV/Local CV for each repeat experiment where a ratio equal to one means that the variation at the local scale is equal to the variation at the global scale. This analysis yielded six ratios: three repeat measurements for the patchy landscape R_p and three repeat measurements for the continuous landscape R_c. To test whether R_p and R_c differed significantly, we used a Wilcoxon rank-sum test.

(iv) Spatial correlation

To calculate the spatial correlation between patches, time traces were used as shown in figure 1, where a single fluorescence time trace represents the dynamics in a single patch. Spatial correlations were calculated as a function of increasing inter-patch distance using the corrcoef function in MATLAB.

(v) Survival analysis

For the survival analysis, we used the fluorescence signal originating from all 98 × 98 subregions in the patches. As is described in the 'Results' section, the typical fluorescence signal rises first (due to bacterial growth) and subsequently reaches a maximum, after which it declines (due to predation). First, the time-point associated with the maximum value in the fluorescence is determined. Second, the time-point at which the fluorescence crosses the cut-off fluorescence value associated with a region that does not contain any bacteria is determined. This time-point is recorded and designated as the 'time-of-death' for that particular region in space. This procedure is repeated for all time traces, and Kaplan–Meier survival curves are generated using the log-rank function of MATLAB. As the patchy- and continuous-habitat experiments were performed in triplicate, we obtained three sets of survival curves (electronic supplementary material, figure), each quantifying the surviving population fractions in the patchy and continuous landscapes over time. The log-rank algorithm determines this fraction, as well as whether the two survival curves for the patchy and continuous landscapes are statistically different, including the associated *p*-value. Additionally,

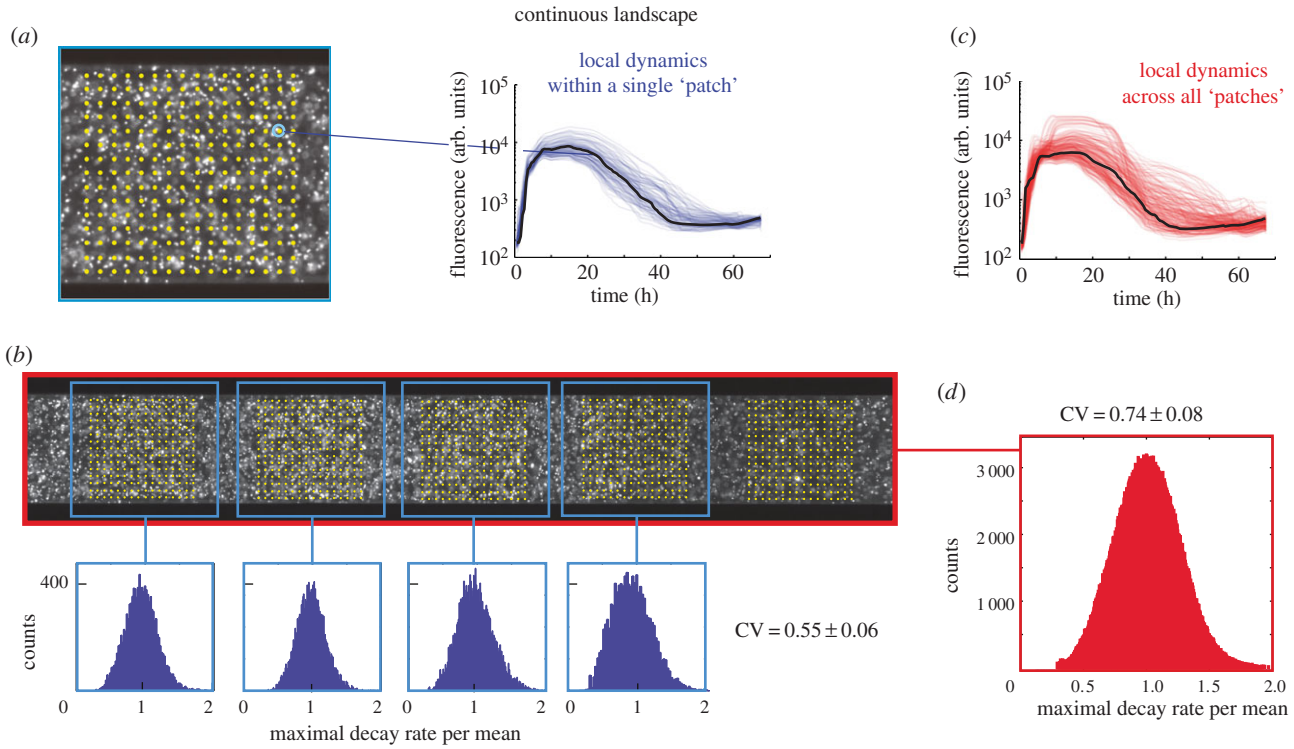

Figure 3. Predation rates in the continuous landscape. (*a*) Yellow dots indicate 98 × 98 points (for clarity, only 16 × 16 are shown) that were used to generate time traces (thin blue lines show single time traces for one virtual patch, the fat black line represents the mean) from patches of the continuous landscape. The maximum predation rate is extracted from individual traces. (*b*) Distribution of the maximal rate of decay of four virtual patches. (*c*) All time traces of all virtual patches within a continuous habitat (thin red lines show single time traces for one patch, the fat black line represents the mean). (*d*) The distributions of the maximum decay rates calculated for all points in all virtual 'patches' within the continuous landscape.

the algorithm determines the residual values, i.e. the population fraction that persists.

The survival analysis as described above was also performed separately for the periphery (the outer rim of the habitat patch, measuring 15 µm or less to the closest sidewall) and centre (the remaining 70 × 70 × 10 μm^3 central volume element) of the habitat patches. The centre of the habitat patches has a low surface to volume ratio (0.20 μm^{-1}) as only a top and bottom surface are present, whereas the periphery is enclosed by the sidewalls increasing the surface to volume ratio (0.28 μm^{-1} and 0.27 μm^{-1} for the patchy and continuous habitats, respectively).

(vi) Real-time movies

Real-time and time-lapse movies provide additional insights beyond those extracted from total fluorescence intensity time traces. For example, movies help to identify different modes of prey growth such as surface-associated growth, which manifests itself as an increase in fluorescence at the edges of an observed microcolony in combination with limited (or even the absence of) motility. Furthermore, the process and timing of predation can be followed. While we are unable to observe the exact time of entry of the predator, we clearly observed the formation of bdelloplasts when rod-shaped prey were converted into round-shaped bdelloplasts, followed by their sudden disappearance due to lysis (electronic supplementary material, movies S1, S4, and S5).

3. Results

Prior to studying the dynamics between predator and prey, we performed a control experiment in which the landscape was only inoculated with prey (figure 1*b*,*c*). This experiment shows that *E. coli* quickly populates the entire landscape, though some spatial variation is present (figure 1*b*). The mean fluorescence intensity of all patches over time (figure 1*c*) shows that the prey initially grows exponentially, until it reaches stationary phase approximately 10 h after inoculation. In the following 30 h, the population did not collapse, as evidenced by an approximately constant mean fluorescent intensity. We conclude that in the absence of predator, and in good agreement with previous studies of *E. coli* in microfabricated landscapes [18,38], the bacterial prey population inoculated in the microfabricated landscape exhibited all the familiar phases of growth and did not show population collapse even after 2 days.

A different picture emerges when predator and prey are both inoculated from opposite sides. Figure 1 shows prey dynamics as a function of space and time in the presence of the predator, for the patchy landscape (figure 1*d*) and for the continuous landscape (figure 1*e*). An experiment is typically characterized by four phases in the predator–prey dynamics (labelled (i) through (iv) in figure 1*d*). Initially, (phase (i)), growth of the prey population is dominant over predation and consequently the population density increases. During phase (i), the majority of *E. coli* bacteria are planktonic, motile, and migrate between patches rapidly, whereas in phase (ii), the majority of *E. coli* become sessile and show an increase in surface-associated growth [16]. Without predator (figure 1*b*,*c*), one observes phases (i) and (ii) only (see [38] for a detailed analysis of the colonization process). When prey and predator are both (simultaneously) inoculated, predation starts to dominate in phases (ii) and (iii) and the population density of *E. coli* starts to decline approximately 10–20 h after inoculation. In the final phase (iv), the prey density reaches a steady-state, where most of the prey population is eradicated, except for a small number of prey that is

Table 1. Local and global coefficients of variation in the patchy and continuous landscape. Values are the mean ± standard error of the mean (s.e.m.) of three independent experiments.

	mean ± s.e.m.	scale	graphical representation
$CV_{l,p}$	0.51 ± 0.06	local	⟨CV⟩ of all patches in patchy landscape
$CV_{g,p}$	1.53 ± 0.66	global	CV of entire patchy landscape
$CV_{l,c}$	0.55 ± 0.06	local	⟨CV⟩ of all 'patches' in continuous landscape
$CV_{g,c}$	0.74 ± 0.08	global	CV of entire continuous landscape

presumably characterized by plastic phenotypic resistance to predation [25]. We note that while the specific spatial pattern, e.g. the presence of two separated predation foci in the patchy landscape in figure 1*d*, varies from experiment to experiment (see electronic supplementary material, figure), all six independent experiments showed the four phases described above. Electronic supplemental material, movie S1, shows the predation process in more detail, including the formation of round bdelloplasts and their sudden disappearance as they get lysed by *B. bacteriovorus*. We conclude that *B. bacteriovorus* do indeed predate *E. coli* populations in the structured landscapes and that the prey population is decimated.

We then asked how habitat topology influences the variation of prey dynamics at local versus global spatial scales. To address this, we first quantified how much the maximal predation rate of the prey population varied *within* patches in the patchy landscape (local scale), where the conditions are presumably uniform, and compared this quantity to the spread of the maximal decay rate *across* patches (global scale). To compare spreads with slightly different means, we used the CV as a measure of the spread (see the 'Image processing and data analysis' section for details). We calculated four values of the CV: (1) $CV_{l,p}$ (local, patchy; variation within patches in the patchy landscape), (2) $CV_{g,p}$ (global, patchy; variation in the entire patchy landscape), (3) $CV_{l,c}$ (local, continuous; variation within the virtual 'patches' in the continuous landscape), and (4) $CV_{g,c}$ (global, continuous; variation in the entire continuous landscape). The values obtained, as well as a schematic of the regions for which the CVs were calculated, are summarized in table 1.

First, we observed that in the patchy landscape the variation within a patch (local scale) was smaller than the variation between patches ($CV_{l,p} < CV_{g,p}$). A statistical comparison of $CV_{l,p}$ and $CV_{g,p}$ is provided below. This observation is consistent with the notion that conditions that affect predator–prey dynamics, for example fluctuations in predator and prey densities, vary across patches in a patchy landscape. The source of the increased variation across the landscape is not obvious as both the limited migration due to the patchiness of the landscape and the increasing physical distance between ever more distant regions could contribute to this result. To uncouple the influences of the patchy structure and physical distance, we compared the patchy landscape to the continuous landscape that does not contain structural patchiness. We found that the local CV of the decay rates within the 'virtual patches' in the continuous landscape, $CV_{l,c}$, is 0.55 ± 0.06, were very similar to the local CV in the patchy landscape ($CV_{l,p} \approx CV_{l,c}$). This similarity is expected since both distributions represent local dynamics within an identical area (and volume) in the landscapes. The maximal decay rates of all time traces across the entire continuous landscape (red traces in figure 3*c*) have a relatively narrow distribution (figure 3*d*) and has a global $CV_{g,c}$ of 0.74 ± 0.08. This number is larger than the average local $CV_{l,c}$ of the 'virtual patches' in the continuous landscape, indicating that conditions in the entire continuous landscape are somewhat more diverse than in a small fraction of the entire landscape. However, it is important to note that the global $CV_{g,c}$ of the continuous landscape is considerably smaller than the global $CV_{g,p}$ of the patchy landscape ($CV_{g,p} = 1.53 \pm 0.66$).

To properly address the question whether the patchiness of the patchy landscape increases variation, we calculated the ratios $R_p = CV_{g,p}/CV_{l,p}$ for the patchy landscape and $R_c = CV_{g,c}/CV_{l,c}$ for the continuous landscape. This assessment shows that R_p is indeed larger than R_c ($R_p = 2.8 \pm 0.9$, $R_c = 1.3 \pm 0.02$ mean ± s.e.m. of $n = 3$ experiments, $R_p > R_c$ $p = 0.05$, using a single-sided Wilcoxon rank-sum test). We may thus conclude that our findings support the hypothesis that patchiness increases the variation in population decay rates of the prey by approximately a factor of two.

While the measurements described above show that patchiness influences the predator–prey interaction at the global level, these measurements do not provide insight into the extent to which the prey dynamics is correlated in space. Spatial correlation gives insights into the connectivity between patches and the ease with which bacteria can move between patches. To quantify this, we analysed the correlation between the time traces of patches as a function of patch distance. Figure 4*a* shows the dependence on distance of the Pearson's correlation coefficient, for the patchy (red) and continuous (black) landscapes (see the 'Spatial Correlation' section). As expected, both landscapes show a decrease in correlation with increasing distance. However, while the two landscapes lose correlation similarly for distances up to approximately 15

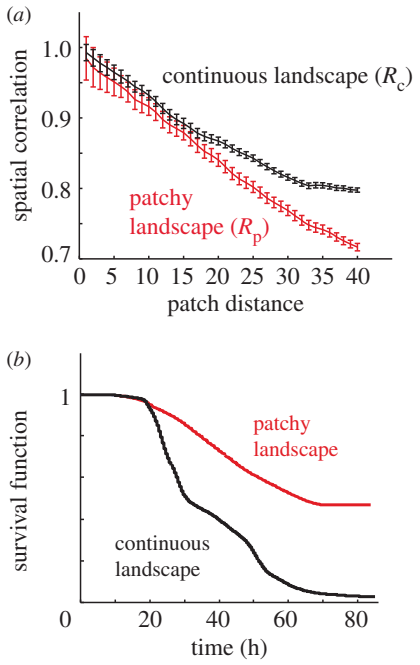

Figure 4. Correlation in patchy and continuous habitats. (*a*) The temporal correlation of the population dynamics decreases with increasing patch distance. Beyond approximately 15 patches, correlation in the patchy landscape (red) is lost more rapidly than in the continuous landscape (black). (*b*) Kaplan–Meier survival functions for a patchy landscape (red) and a continuous landscape (black). The two functions differ ($p < 0.00001$) and the fraction of prey population that remains in the patchy landscape is higher than in the continuous landscape ($p = 0.05$), see Results.

patches, this analysis also shows that the patchy landscape loses correlation faster than the continuous landscape beyond 15 patches. Spatial dynamics in the patchy landscape thus extend beyond a single patch, yet are correlated over shorter distances than in the continuous landscape, a high migration rate of bacteria between adjacent patches in the initial phases of the experiment may explain correlations beyond the patch size. A high migration rate between patches would be expected to contribute to a high coupling between patches and synchronization in the dynamics between patches. Indeed, real-time movies of the initial phases of the experiment (electronic supplementary material, movies S2 and S3) show that up to hundreds of bacteria can migrate between patches per minute, depending on bacterial density. This finding suggests that the migration rate in the patchy landscape is apparently sufficiently high to generate correlation in the dynamics between a few adjacent patches, but over long (more than 15 patches) distances, the effects of the patchy landscape on the dynamics become apparent. As such, the present spatial configuration represents an unexplored intermediate regime between a coherent well-mixed state and an entirely fragmented state [12].

Given our finding that patchiness affects variation and spatial correlation of the prey dynamics, we then asked what the ramifications of these findings were for the survival of prey. Does patchiness, like in various macroscopic systems [5,8,12,13] give rise to an increased persistence of the prey population, or do specific bacterial properties (such as high mobility, high density, and surface growth) render the analogy to macroscopic organisms invalid? To answer this question, we performed a survival analysis for prey in both the patchy and continuous landscapes. Using fluorescence as a proxy for prey persistence, we generated survival curves representing the spatial fraction of the prey population that survives (see figure 4*b* and the 'Survival Analysis' section for details). After the onset of predation (in this experiment approx. after 10 h), survival curves in both the patchy and continuous landscape start to decline. Interestingly, the survival functions of the patchy and continuous populations are not equal, ($p < 0.00001$ using a log-rank test). Survival curves for all the experiments are displayed in electronic supplementary material, figures *g–i*. These results show that while almost the entire population dies in the continuous landscape (residual value $= 0.04 \pm 0.04$, $n = 3$), a significant fraction of the population in the patchy landscape survives (0.36 ± 0.10, $n = 3$) demonstrating that prey survival in the patchy landscape is increased compared with the continuous landscape ($p = 0.05$, using a single-sided Wilcoxon rank-sum test). The increased survival in the patchy landscape is not caused by a lower *per capita* predation rate as the absolute values for the *per capita* predation rates are 0.06 ± 0.01 and 0.05 ± 0.01 per hour for the patchy geometry and continuous landscapes, respectively, in good agreement with previously measured batch values [30–32]. This control shows that (i) the geometry of the landscape does not influence the kinetics of the predator–prey interaction and that (ii) the rates measured in the microchip are comparable to those previously measured.

4. Discussion

This work was inspired by studies on macro-scale patchy landscapes showing that patchiness can greatly impact the spatio-temporal dynamics of predator–prey systems, such as an extended lifetime of a macroscopic population [8–11]. We investigated to what extent bacterial predator–prey systems in microfragmented landscapes exhibit similar behaviours. The present patchy landscape can be considered 'mildly' fragmented as on the one hand fragmentation increases the variation in predation rates, but on the other hand spatial correlations extend over multiple patches. The presence of this intermediate regime should perhaps be considered in the context of the fundamental differences between macroscopic animals inhabiting macroscopic landscapes and microscopic organisms inhabiting microscopic landscapes. First, compared to macroscopic animals, bacteria (and especially *B. bacteriovorus*) move through space fast and grow to high densities. If one were to simply scale up the microfragmented landscape and its microbial inhabitants to macroscopic proportions, one would obtain the following (rather absurd) large-scale animal equivalent: hundreds of cheetahs racing at approximately 500 km h^{-1} in random directions while hunting a few hundred antelopes that run around at 100 km h^{-1} in a square field of only 100×100 m. Such exceedingly high density and mobility would likely give rise to relatively homogeneous spatial dynamics within the field and result in spatial correlations that extend beyond it. Moreover, bacteria can adopt distinct lifestyles, existing as individual planktonic cells that swim freely, or growing as multi-cellular surface-associated colonies. Bacteria exhibiting one of these two lifestyles differ in a myriad of ways including cellular mobility, capacity to forage, resistance to environmental insults, and physiology. By impacting core processes like colonization, survival, and extinction, lifestyle switching plays a central role in

bacterial ecology. Another distinction between the microscopic and macroscopic worlds is that signalling molecules, nutrients, and waste diffuse across space highly efficiently. For example, a small molecule such as glucose traverses the length of a patch (100 µm) in approximately 10 s and a distance of 15 patches in approximately an hour (which is in the order of one bacterial division time). Such environmental homogenization may be less apparent for macroscopic animals. A future theory of microbial ecology that draws from macroscopic theory would have to take into account these fundamental differences.

Perhaps the most salient effect described in this manuscript is the observation that a significant fraction of prey in the fragmented landscape persists, in contrast to the prey population in the continuous landscape that is nearly eradicated (surviving prey population fraction of 0.04 ± 0.04 $n = 3$). As this effect cannot be attributed to a difference in predation rates (the maximal predation rates in the two landscapes are equal), the increased persistence may be attributed to the geometry of the patchy landscape. Classical metapopulation dynamics, in which a given patch becomes extinct after which it is 'rescued' by migration of prey from an adjacent patch, could be responsible for the increased survival in the patchy landscape. However, while this scenario cannot be ruled out completely, the limited extent to which lateral movement (migration) is visible in the kymographs leads us to favour a different explanation.

Previous work has shown that while *B. bacteriovorus* can predate an *E. coli* biofilm, a significant fraction of the biofilm often remains [39], in contrast to predation on planktonic *E. coli* cultures where only a minute fraction of the population survives due to phenotypic resistance. In the microhabitats under investigation here, part of the prey population grows as a surface-associated biofilm (see electronic supplementary material, movies S1, S4, and S5). Surface-associated growth concentrates in the periphery of habitat patches where, due to the presence of sidewalls, the surface to volume ratio is higher when compared with the centre of habitat patches. An increase in the population fraction adopting a surface-associated lifestyle may render it more resistant to predation and could result in an increased survival in the periphery of patches. To test this hypothesis, we performed a survival analysis for the periphery and centre of habitat patches separately. This analysis revealed that prey persistence in the patchy habitat is indeed significantly higher in the periphery compared with the centre of patches (peripheral residual fraction of 0.49 ± 0.14, versus 0.30 ± 0.10, $p < 0.02$ using a one-tailed paired *t*-test). In contrast, we did not observe a significant difference when comparing survival in the periphery and centre of (virtual) patches in the continuous habitat (0.05 ± 0.05 and 0.04 ± 0.05, respectively). Two effects may explain the difference observed between the patchy and continuous habitats: (i) patches in a patchy habitat have four sidewalls, whereas (virtual) patches in the continuous habitat only have two, lowering the surface to volume ratio and (ii) patches in a patchy habitat have corners facilitating bacterial adhesion [40], while corners are absent in the continuous habitat. Both the increase in surface to volume ratio and the presence of corners facilitate surface-associated growth. As a result, geometry-induced enhancement of surface-associated growth may be responsible for the increased persistence of prey we observe in the patchy habitat. While in our experiments the persisting bacteria did not divide, the exact physiological state of these remaining bacteria remains unknown. Assessing the capacity of these persisting prey to grow and divide will be of importance when using *B. bacteriovorus* for water cleaning, crop protection, and as an additional means to fight bacterial infections.

Authors' contributions. F.J.H.H., E.J., C.D., and D.A.K. conceived and designed the experiments. F.J.H.H. and D.A.K. performed experiments and analysed the data. O.R. designed and contributed protocols. F.J.H.H. and D.A.K. wrote the manuscript. All authors read and approved the final manuscript.

Competing interests. We have no competing interests.

Funding. Supported by grants from the Minerva Foundation for Movement Ecology and the Dean of the faculty of Science of the Hebrew University to D.A.K. European Research Council grant NanoforBio No. 247072 and the Netherlands Organisation for Scientific Research (NWO/OCW) as part of the Frontiers of Nanoscience programme to C.D.

Acknowledgements. We thank Prof. Ran Nathan, Prof. Nadav Shnerb, Dr R.W. Koster, Prof. Liz Sockett, and several anonymous reviewers (from several journals) for insightful comments.

References

1. Dethlefsen L, Eckburg PB, Bik EM, Relman DA. 2006 Assembly of the human intestinal microbiota. *Trends Ecol. Evol.* **21**, 517–523. (doi:10.1016/j.tree.2006.06.013)
2. Stocker R. 2012 Marine microbes see a sea of gradients. *Science* **338**, 628–633. (doi:10.1126/science.1208929)
3. Ngom NF, Garnier P, Monga O, Peth S. 2011 Extraction of three-dimensional soil pore space from microtomography images using a geometrical approach. *Geoderma* **163**, 127–134. (doi:10.1016/j.geoderma.2011.04.013)
4. Wolf AB, Vos M, de Boer W, Kowalchuk GA. 2013 Impact of matric potential and pore size distribution on growth dynamics of filamentous and non-filamentous soil bacteria. *PLoS ONE* **8**, e83661. (doi:10.1371/journal.pone.0083661)
5. Tilman D, Kareiva PM. 1997 *Spatial ecology: the role of space in population dynamics and interspecific interactions*. Princeton, NJ: Princeton University Press.
6. Durrett R, Levin S. 1994 The importance of being discrete (and spatial). *Theor. Popul. Biol.* **46**, 363–394. (doi:10.1006/tpbi.1994.1032)
7. Hanski I, Gaggiotto O. 2004 *Ecology, genetics, and evolution of metapopulations*. London, UK: Elsevier Academic Press.
8. Holyoak M, Lawler SP. 1996 Persistence of an extinction-prone predator–prey interaction through metapopulation dynamics. *Ecology* **77**, 1867–1879. (doi:10.2307/2265790)
9. Dey S, Joshi A. 2006 Stability via asynchrony in Drosophila metapopulations with low migration rates. *Science* **312**, 434–436. (doi:10.1126/science.1125317)
10. Sutcliffe OL, Thomas CD, Yates TJ, Greatorex-Davies JN. 1997 Correlated extinctions, colonizations and population fluctuations in a highly connected ringlet butterfly metapopulation. *Oecologia* **109**, 235–241. (doi:10.1007/s004420050078)
11. Ellner SP *et al.* 2001 Habitat structure and population persistence in an experimental community. *Nature* **412**, 538–543. (doi:10.1038/35087580)
12. Earn DJD, Levin SA, Rohani P. 2000 Coherence and conservation. *Science* **290**, 1360–1364. (doi:10.1126/science.290.5495.1360)
13. Ben Zion Y, Yaari G, Shnerb NM. 2010 Optimizing metapopulation sustainability through a

checkerboard strategy. *PLoS Comput. Biol* **6**, e1000643. (doi:10.1371/journal.pcbi.1000643)
14. Berg HC. 2000 Motile behavior of bacteria. *Phys. Today* **53**, 24–29. (doi:10.1063/1.882934)
15. Männik J, Driessen R, Galajda P, Keymer JE, Dekker C. 2009 Bacterial growth and motility in sub-micron constrictions. *Proc. Natl Acad. Sci. USA* **106**, 14 861–14 866. (doi:10.1073/pnas.0907542106)
16. Hall-Stoodley L, Costerton JW, Stoodley, P. 2004 Bacterial biofilms: from the natural environment to infectious diseases. *Nat. Rev. Microbiol.* **2**, 95–108. (doi:10.1038/nrmicro821)
17. Drescher K, Shen Y, Bassler BL, Stone HA. 2013 Biofilm streamers cause catastrophic disruption of flow with consequences for environmental and medical systems. *Proc. Natl Acad. Sci. USA* **110**, 4345–4350. (doi:10.1073/pnas.1300321110)
18. Keymer JE, Galajda P, Muldoon C, Park S, Austin RH. 2006 Bacterial metapopulations in nanofabricated landscapes. *Proc. Natl Acad. Sci. USA* **103**, 17 290–17 295. (doi:10.1073/pnas.0607971103)
19. Connell JL, Ritschdorff ET, Whiteley M, Shear JB. 2013 3D printing of microscopic bacterial communities. *Proc. Natl Acad. Sci. USA* **110**, 18 380–18 385. (doi:10.1073/pnas.1309729110)
20. Hol FJH, Dekker C. 2014 Zooming in to see the bigger picture: microfluidic and nanofabrication tools to study bacteria. *Science* **346**, 1251821. (doi:10.1126/science.1251821)
21. Hol FJH, Hubert B, Dekker C, Keymer JE. 2015 Density-dependent adaptive resistance allows swimming bacteria to colonize an antibiotic gradient. *ISME J.* **10**, 30–38. (doi:10.1038/ismej.2015.107)
22. Lambert C, Evans KJ, Till R, Hobley L, Capeness M, Rendulic S, Schuster SC, Aizawa S-I, Sockett RE. 2006 Characterizing the flagellar filament and the role of motility in bacterial prey-penetration by *Bdellovibrio bacteriovorus*. *Mol. Microbiol.* **60**, 274–286. (doi:10.1111/j.1365-2958.2006.05081.x)
23. Sockett RE. 2009 Predatory lifestyle of *Bdellovibrio bacteriovorus*. *Annu. Rev. Microbiol.* **63**, 523–539. (doi:10.1146/annurev.micro.091208.073346)
24. Fenton AK, Lambert C, Wagstaff PC, Sockett RE. 2010 Manipulating each MreB of *Bdellovibrio bacteriovorus* gives diverse morphological and predatory phenotypes. *J. Bacteriol.* **192**, 1299–1311. (doi:10.1128/JB.01157-09)
25. Shemesh Y, Jurkevitch E. 2004 Plastic phenotypic resistance to predation by *Bdellovibrio* and like organisms in bacterial prey. *Environ. Microbiol.* **6**, 12–18. (doi:10.1046/j.1462-2920.2003.00530.x)
26. Kim E-H, Dwidar M, Mitchell RJ, Kwon Y-N. 2013 Assessing the effects of bacterial predation on membrane biofouling. *Water Res.* **47**, 6024–6032. (doi:10.1016/j.watres.2013.07.023)
27. Sockett RE, Lambert C. 2004 *Bdellovibrio* as therapeutic agents: a predatory renaissance? *Nat. Rev. Microbiol.* **2**, 669–675. (doi:10.1038/nrmicro959)
28. Fratamico P, Whiting R. 1995 Ability of *Bdellovibrio bacteriovorus* 109 J to lyse Gram-negative food-borne pathogenic and spoilage bacteria. *J. Food Prot.* **58**, 160–164.
29. Fratamico PM, Cooke PH. 1996 Isolation of Bdellovibrios that prey on *Eschericha coli* O157:H7 and Salmonella species and application for removal of prey from stainless steel surfaces. *J. Food Saf.* **16**, 161–173. (doi:10.1111/j.1745-4565.1996.tb00157.x)
30. Lambert C, Smith MCM, Sockett RE. 2003 A novel assay to monitor predator-prey interactions for *Bdellovibrio bacteriovorus* 109 J reveals a role for methyl-accepting chemotaxis proteins in predation. *Environ. Microbiol.* **5**, 127–132. (doi:10.1046/j.1462-2920.2003.00385.x)
31. Jurkevitch E, Minz D, Ramati B, Barel G. 2000 Prey range characterization, ribotyping, and diversity of soil and rhizosphere *Bdellovibrio* spp. isolated on phytopathogenic bacteria. *Appl. Environ. Microbiol.* **66**, 2365–2371. (doi:10.1128/AEM.66.6.2365-2371.2000)
32. Stolp H, Starr MP. 1963 *Bdellovibrio bacteriovorus* gen. et sp. n., a predatory, ectoparasitic, and bacteriolytic microorganism. *Antonie Van Leeuwenhoek* **29**, 217–248. (doi:10.1007/BF02046064)
33. Shanks RMQ, Davra, VR, Romanowski, EG, Brothers KM, Stella NA, Godboley D, Kadouri DE. 2013 An eye to a kill: using predatory bacteria to control Gram-negative pathogens associated with ocular infections. *PLoS ONE* **8**, e66723. (doi:10.1371/journal.pone.0066723)
34. Monnappa AK, Dwidar M, Seo JK, Hur J-H, Mitchell RJ. 2014 *Bdellovibrio bacteriovorus* inhibits *Staphylococcus aureus* biofilm formation and invasion into human epithelial cells. *Sci. Rep.* **4**, 3811. (doi:10.1038/srep03811)
35. Hol FJH, Galajda P, Nagy K, Woolthuis RG, Dekker C, Keymer JE. 2013 Spatial structure facilitates cooperation in a social dilemma: empirical evidence from a bacterial community. *PLoS ONE* **8**, e77042. (doi:10.1371/journal.pone.0077042)
36. Edelstein A, Amodaj N, Hoover K, Vale R, Stuurman N. 2010 Computer control of microscopes using μManager. *Curr. Protoc. Mol. Biol.* Chaper 14: 14.20.1–14.20.17. (doi:10.1002/0471142727.mb1420s92)
37. Park S, Kim D, Mitchell RJ, Kim T. 2011 A microfluidic concentrator array for quantitative predation assays of predatory microbes. *Lab. Chip* **11**, 2916–2923. (doi:10.1039/C1LC20230H)
38. van Vliet S, Hol FJH, Weenink T, Galajda P, Keymer JE. 2014 The effects of chemical interactions and culture history on the colonization of structured habitats by competing bacterial populations. *BMC Microbiol.* **14**, 116. (doi:10.1186/1471-2180-14-116)
39. Kadouri DE, O'Toole GA. 2005 Susceptibility of biofilms to *Bdellovibrio bacteriovorus* attack. *Appl. Env. Microbiol.* **71**, 4044–4051. (doi:10.1128/AEM.71.7.4044-4051.2005)
40. Friedlander RS, Vlamakis H, Kim P, Khan M, Kolter R, Aizenberg J. 2013 Bacterial flagella explore microscale hummocks and hollows to increase adhesion. *Proc. Natl Acad. Sci. USA* **110**, 5624–5629. (doi:10.1073/pnas.1219662110)